Supplement of Atmos. Meas. Tech., 11, 2653–2668, 2018
https://doi.org/10.5194/amt-11-2653-2018-supplement

Atmospheric Measurement Techniques
Open Access
EGU

Supplement of

How well can global chemistry models calculate the reactivity of short-lived greenhouse gases in the remote troposphere, knowing the chemical composition

Michael J. Prather et al.

Correspondence to: Michael J. Prather (mprather@uci.edu)

Introduction

This work focuses on the reactivity of tropospheric air parcels, adopting a unique protocol to test the photochemical modules of the 3-D models, including regional-to-global chemistry-transport models, chemistry climate models, and Earth system models. The protocol was designed to enable 3-D models to ingest a stream of 1 s to 10 s (0.2 - 2 km) in situ detailed chemistry measurements from an aircraft campaign. The protocol embeds these parcels in a unique, appropriate grid cell of each model, turns off processes that mix adjacent grid cells, and integrates the 3-D model for 24 hours. The photochemical module is thus dependent only on the chemical mechanism and the diurnal cycle of photolysis rates, which are driven in turn by temperature, water vapor, solar zenith angle, clouds, possibly aerosols and overhead ozone, which are calculated as they would be in each model. This is based on the A-runs of the 3-D models demonstrated in Prather et al. (2017, hence P2017)

Reactivities

The definition of reactivity and the chemical rates used to evaluate them are based on the ACP paper that began this approach (P2017). Reactivity is defined here as the 24-hour average rate of important compounds, which here are production and loss of tropospheric ozone and methane.

Loss of CH_4 (L-CH4, ppb/day) is calculated from the OH reaction in the troposphere (Cl reactions are not included because the species needed to define them are not readily measured):

$$CH_4 + OH \rightarrow CH_3 + H_2O \qquad (1)$$

Production of O_3 (P-O3, ppb/day) is calculated from the peroxy radical reactions with NO as well as photolysis of O_2 in the upper tropical troposphere (mostly above 12 km, so not relevant for DC-8 aircraft measurements):

$$HO_2 + NO \rightarrow NO_2 + OH \qquad (2a)$$
$$RO_2 + NO \rightarrow NO_2 + RO \qquad (2b)$$
$$\text{followed by } NO_2 + h\nu \rightarrow NO + O \text{ and } O + O_2 \rightarrow O_3 \qquad (2c)$$
$$O_2 + h\nu \rightarrow O + O \text{ (times 2)} \qquad (2d)$$

Loss of O_3 (L-O3, ppb/day) is based on three reactions with HOx radicals or water:

$$O_3 + OH \rightarrow O_2 + HO_2 \qquad (3a)$$
$$O_3 + HO_2 \rightarrow HO + O_2 + O_2 \qquad (3b)$$
$$O(^1D) + H_2O \rightarrow OH + OH \qquad (3c)$$
$$\text{originating from } O_3 + h\nu \rightarrow O(^1D) + O_2 \qquad (3d)$$

In highly polluted conditions there are additional reactions involving nitrate compounds or direct reaction with alkenes or isoprene that lead to O_3 loss. These diagnostics were designed for the remote troposphere and are adequate for calculating the true P-O3 and L-O3. In tests with the A-runs (P2017), the diagnosed P-O3 minus L-O3 matched the 24-hour change in O_3.

Protocol

The data stream includes key species determining tropospheric chemistry that need to be initialized in the 3-D models: O_3, NOx (=NO+NO_2), HNO_3, HNO_4, PAN (peroxyacetyl nitrate), RNO_3 (CH_3NO_3 and all alkyl nitrates), HOOH, ROOH (CH_3OOH and smaller contribution from C_2H_5OOH), HCHO, CH_3CHO (acetaldehyde), C_3H_6O (acetone), CO, CH_4, C_2H_6, alkanes (all C_3H_8 and higher), alkenes (all C_2H_4 and higher), aromatics (benzene, toluene, xylene), C_5H_8 (isoprene plus terpenes), plus temperature (T) and specific humidity (q). When a specified species includes a collective (e.g., NOx, aromatics) each model can partition that collective total mole fraction in similar proportions to those as calculated in the model. The algorithm for dealing with missing species or an over-specified class of species is truly model dependent. For example, the UCI model has a simple approximation and single class for all aromatics and consolidates emissions of benzene, toluene, and xylene into 'aromatics' that react as benzene. The NCAR model includes all three species explicitly, and thus they will take the mole fraction of 'aromatics' and partition it into benzene, toluene, and xylene, scaled to their values in the grid cell that is being overwritten with the UCI data stream.

This synthetic data stream is taken from an earlier UCI model version running at high resolution (~0.55 degrees horizontal, and ~0.5 km vertical). All the model grid cells from 0.5 to 12 km from 60S to 60N along 3 adjacent meridians at 180W were used (14,880 parcels). The choice of dropping points below 0.5 km was made earlier to avoid the highly polluted boundary layer over land sources, but when the experiment chose to focus on the middle Pacific, this exclusion was no longer necessary. The protocol was already in process and some model results completed, so the altitude cut off was left. It will clearly not be used with the ATom measurement data stream (ATom, 2017) in subsequent papers since there is extensive data from the marine boundary layer taken at 0.16 km altitude. No attempt was made to follow ATom-like profiling. The overall set of 14880 points from 60S to 60N in the data stream presents a dense climatology and tests the ability of the 3-D models to treat fine-resolution data.

Each data stream record includes latitude, longitude, and pressure, which are used to assign the closest model grid cell to each simulated air parcel. The model's restart file for one of the 5 days in August (8/01, 8/06, 8/11, 8/16, 8/21) is overwritten with the simulated chemical species at the appropriate grid cell. When two parcels fall within the same grid cell, an algorithm shifts the longitude of the second parcel to a nearby cell. Each model runs this restart file for 1 day using the A-run protocol, which keeps all air parcels isolated with little influence from neighboring grid cells. (These neighbor cells may be either from the simulated data or the original restart file.) The use of such modified restart files allows for ready calculation of the reactivities in global models as per the A-runs of P2017.

In the analysis here, each of the data stream parcels is weighted equally to simplify this analysis; but for an observed data stream, each parcel must be weighted separately to ensure uniform sampling of tropospheric mass, particularly the profiles.

Less useful diagnostics and problems with the protocol

The slope of parcel reactivities relative to the reference case indicates bias that changes from low to high reactivity and may be useful in diagnosing the chemical models. Most of the slopes in Table S3 lie within 1±0.08 (bold text), and these combinations have mostly been identified earlier. The slope does identify a disagreement across the reference-case models: for J-NO2, GSFC 's slope is 0.91 while UCI's is 1.13; these biases are symmetric because both have averaged with GC (slope = 0.97) to get the reference case.

Correlation coefficients of parcels for model pairs are also calculated (not shown); but these are all large, usually 0.9 or greater; and do not provide any insight on model differences. There are large differences in reactivities associated with latitude (sun angle and length of day) and with pressure, and the models reproduce these first-order effects.

The GFDL and NCAR CCMs could not maintain the fixed, data-stream T&q values over the 24-hour integration, which leads to larger rms differences because reactivities depend on both T and especially q. This explains in part why the GFDL and NCAR models in Figure 2 have larger scatter for reactivities than the other non-GISS models, but similar scatter in J values. This effect may also contribute to the larger day-to-day rms, for NCAR at least, and is examined more extensively with the UCI CTM running with the T&q's from both models (Section 3.5).

Tables

Table S1a. Participating models

model		year & days simulated	updates, references	email
GFDL	AM3	2013 Aug 1-6-11-16-21	*Horowitz et al., 2003; Li et al., 2017.*	amfiore @ldeo.columbia.edu
GISS	GISS-E2.1	2013 Aug 1-6-11-16-21	Updated code base to E2.1 and switched to nudging to MERRA [*Rienecker et al.*, 2011]	lee.murray @rochester.edu
GSFC	GMI-CTM	2016 Aug 1-6-11-16-21	*Strahan et al., 2013; Duncan et al., 2007.*	Sarah.A.Strode @nasa.gov
GC	GEOS-Chem	2013 Aug 1-6-11-16-21	v11_01 (using MERRA-2 reanalysis [*Gelaro et al.*, 2017]	lee.murray @rochester.edu
NCAR	CAM4-Chem	2008 Aug 2-6-11-16-21	*Tilmes et al., 2016*	lamar@ucar.edu
UCI	UCI-CTM	2016 Aug 1-6-11-16-21	*Holmes et al, 2013; Prather 2015*; plus aerosol impacts on J and k (v72d), run with observed O_3 climatology	mprather@uci.edu

Table S1b. Model heritage for tropospheric photochemistry

	Chemical Mechanism	Photolysis rates
GFDL	MOZART-2	Fast-J
GISS	CBM-4/RACM (*Houweling et al., 1998; Shindell et al., 2013*). No aromatics.	Fast-J2
GSFC	Combo Strat-Trop; Trop from GEOS-Chem	Fast-JX
GC	GEOS-Chem (http://www.geos-chem.org) v11_01 "standard" mechanism. No MeONO2.	Fast-JX v7.0
NCAR	MOZART v4	TUV lookup tables (*Madronich, 1987*)
UCI	*Prather & Hsu, 2010*, 24 species + Linoz v3	Cloud-J v7.5, full cloud treatment, Fast-J core

Table S2. Slope of each model vs. ref model (5d means)

model	P-O3	L-O3	L-CH4	J-NO2	J-O1D
GFDL	0.91	**0.61**	0.81	0.93	0.93
GISS	**1.48**	**1.47**	**0.32**	1.06	**1.43**
GSFC	0.99	0.99	0.98	0.91	1.00
GC	0.99	0.99	1.00	0.96	0.97
NCAR	0.98	0.90	0.92	0.95	1.10
UCI	1.02	1.01	1.01	1.13	1.03
U2015	*1.02*	*1.02*	*1.02*	*1.12*	*1.03*
U1997	*1.02*	*1.03*	*1.02*	*1.15*	*1.04*
Slopes outside of 1±0.2 are **boldened**. Alternate UCI years are in *italics.*					

Table S3. Slopes for each day vs. 5-day mean for individual models					
all models	P-O3	L-O3	L-CH4	J-NO2	J-O1D
mean ± sd	1±0.03	1±0.04	1±0.04	1±0.09	1±0.02
begin: 1 Aug	1.01	1.01	1.01	1.12	1.02
end: 21 Aug	0.97	0.96	0.96	0.87	0.97

Table S4. Percent of total integrated reactivity in top X% of parcels				
P-O3	5%	10%	25%	50%
GFDL	14	26	52	81
GISS	14	25	51	80
GSFC	13	24	50	79
GC	15	26	53	82
NCAR	14	25	52	81
UCI	15	26	53	82
U2015	*15*	*26*	*53*	*82*
U1997	*15*	*26*	*53*	*82*
L-O3	5%	10%	25%	50%
GFDL	18	32	63	90
GISS	14	26	53	82
GSFC	14	26	54	84
GC	14	26	53	83
NCAR	14	26	53	82
UCI	15	26	54	83
U2015	*15*	*27*	*54*	*84*
U1997	*15*	*27*	*54*	*84*
L-CH4	5%	10%	25%	50%
GFDL	14	26	54	83
GISS	11	20	43	72
GSFC	14	26	55	84
GC	14	26	54	84
NCAR	13	25	53	84
UCI	14	26	54	84
U2015	*14*	*26*	*54*	*84*
U1997	*14*	*26*	*55*	*84*

Table S5. % of total reactivity in top X% of parcels in UCI				
P-O3	5%	10%	25%	50%
1-Aug	15	27	54	83
6-Aug	15	27	54	83
11-Aug	15	27	54	82
16-Aug	14	26	52	81
21-Aug	14	26	52	80
L-O3	5%	10%	25%	50%
1-Aug	15	27	55	85
6-Aug	15	27	55	85
11-Aug	15	27	54	83
16-Aug	15	26	54	83
21-Aug	14	26	52	82
L-CH4	5%	10%	25%	50%
1-Aug	15	27	56	85
6-Aug	15	27	56	85
11-Aug	14	26	55	84
16-Aug	14	26	54	83
21-Aug	14	25	53	83

Table S6. Overlap (%) of the top X% of reactivities vs reference case, all 5-day means			
5%	P-O3	L-O3	L-CH4
GFDL	74	33	44
GISS	61	75	30
GSFC	92	88	86
GC	92	87	88
NCAR	78	40	41
UCI	93	85	84
U2015	90	82	84
U1997	89	82	82
10%			
GFDL	82	58	64
GISS	72	84	34
GSFC	94	92	92
GC	94	92	91
NCAR	81	54	55
UCI	95	88	88
U2015	92	87	85
U1997	91	86	86
25%			
GFDL	90	75	80
GISS	83	88	54
GSFC	97	95	96
GC	97	94	95
NCAR	89	74	77
UCI	97	95	95
U2015	96	92	93
U1997	96	93	93
50%			

GFDL	96	90	93
GISS	88	97	83
GSFC	98	99	99
GC	98	98	99
NCAR	95	89	92
UCI	98	99	99
U2015	98	99	99
U1997	98	98	98

Table S7. Overlap (%) of the top X% of reactivities: 5 days vs 5-day mean for each model

	GSFC			UCI			GC			NCAR		
	P-O3	L-O3	L-CH4	P-O3	L-O3	L-CH4	P-O3	L-O3	L-CH4	P-O3	L-O3	L-CH4
	5%											
08/01	84	76	76	90	84	83	88	83	86	79	50	47
08/06	83	85	84	90	84	82	88	83	87	76	47	50
08/11	87	76	66	90	83	72	91	88	89	81	64	53
08/16	85	85	84	92	85	83	89	82	87	84	68	54
08/21	84	78	73	91	80	75	88	75	76	75	55	49
	10%											
08/01	88	84	83	91	88	88	90	89	88	82	62	60
08/06	85	90	87	91	88	88	90	87	89	83	58	60
08/11	89	82	80	92	85	83	91	91	91	84	66	63
08/16	88	86	86	92	89	87	92	91	91	85	72	67
08/21	88	85	83	91	85	83	89	84	83	81	62	64
	25%											
08/01	92	90	92	94	92	92	95	89	89	90	83	84
08/06	93	94	94	96	93	93	95	93	93	90	76	80
08/11	93	93	94	94	92	92	95	92	94	90	81	84
08/16	95	95	95	97	94	94	95	93	94	91	83	85
08/21	93	94	95	93	92	91	94	90	89	87	75	79
	50%											
08/01	97	99	98	97	98	98	97	97	97	95	93	95
08/06	97	99	98	98	97	97	98	98	98	94	92	93
08/11	96	99	98	98	99	99	97	98	98	96	93	94
08/16	96	98	98	98	99	99	97	98	98	96	92	93
08/21	96	98	98	97	98	98	97	98	98	94	90	92

Table S8. Average and RMS parcel differences for several UCI sensitivity studies. for some case the reference is a 5-day simulation and for others it is a single day (8/16).

	average difference					rms difference				
model	P-O3 ppb/d	L-O3 ppb/d	L-CH4 ppb/d	J-NO2 e-3 /s	J-O1D e-5 /s	P-O3 ppb/d	L-O3 ppb/d	L-CH4 ppb/d	J-NO2 e-3 /s	J-O1D e-5 /s
UCI 2016 5 days	*0.827*	*1.467*	*0.648*	*4.705*	*1.224*					
UCI 2015	0.006	0.007	0.003	0.020	0.003	0.056	0.123	0.058	0.329	0.077
UCI 1997	0.006	0.004	0.001	0.019	0.007	0.057	0.121	0.057	0.334	0.082
fixed solar declin.	0.000	0.000	0.001	0.002	0.000	0.003	0.007	0.003	0.014	0.005
different restart	0.000	0.000	0.000	0.000	0.000	0.006	0.002	0.002	0.000	0.000
UCI 2016 16 Aug	*0.835*	*1.492*	*0.660*	*4.800*	*1.239*					
initialize at 1200H	0.010	0.015	0.003	0	0	0.030	0.017	0.006	0.003	0.001
+ GFDL T	0.005	-0.001	-0.001	-0.001	0.000	0.070	0.050	0.049	0.015	0.018

+ GFDL T&q	0.013	-0.011	-0.009	-0.001	0.000	0.126	0.845	0.297	0.015	0.018
+ NCAR T	0.032	0.015	0.014	0.002	0.004	0.138	0.076	0.074	0.019	0.022
+ NCAR T&q	0.048	0.165	0.061	0.002	0.004	0.198	0.989	0.364	0.019	0.022

Table S9. Differences between modeled and specified T&q over the 5 days		
model	GFDL	NCAR
mean T (K)	-0.11	+0.17
rms T (K)	3.46	3.69
mean $\log_{10}$[q (g/kq)]	-0.02	+0.01
rms $\log_{10}$[q (g/kq)]	0.39	0.41
The other 4 models used the data stream T&q		

Figures

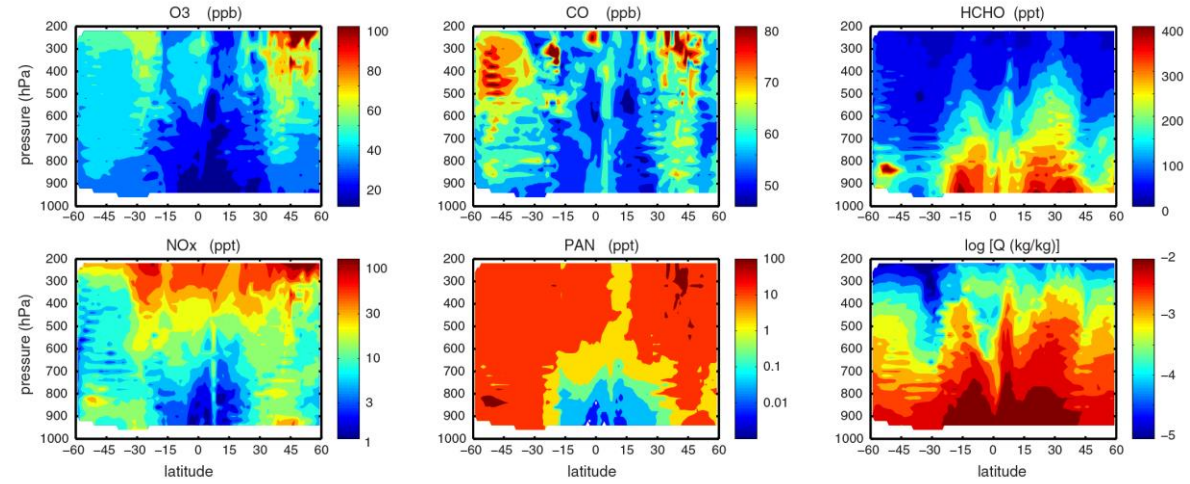

Figure S1. Latitude by pressure plots of 6 key species from the data stream used in this study. The data stream was take from an older version of the UCI CTM running at a grid resolution 640x320 with about 30 layers in the troposphere. Sampling was only for 0.5 to 12 km (960 to 200 hPa).

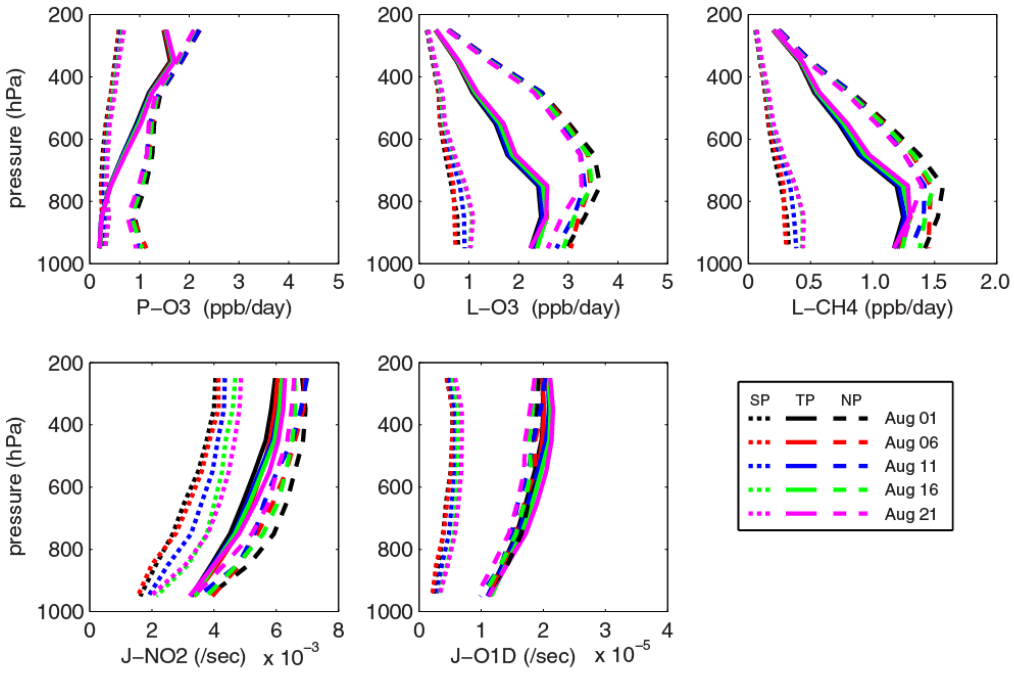

Figure S2. 5 August days of UCI modeled profiles of reactivities (a, P-O3; b, L-O3; c, L-CH4; all ppb/day) and photolysis rates (d, J-NO2; e, J-O1D; all /sec) calculated for the data stream of 14,880 air parcels. Dates are identified by color (black, 08/01; red, 08/06; blue, 08/11; green, 08/16; magenta, 08/21). Latitude bands are identified by line style (solid, 20S-20N; dotted, 50S-20S; dashed, 20N-50N). All parcels are weighted equally.

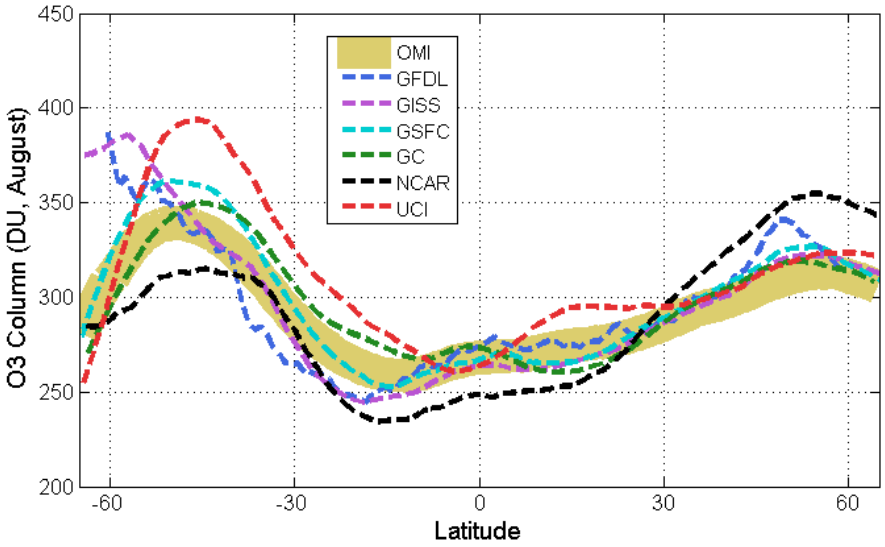

Figure S3. Total O3 columns (DU, August zonal mean) from the models (thick colored lines) and Aura OMI observations (2010-2017, thin black lines). N.B. AM3 is just from 5-day mean of ATom-sim points at dateline.

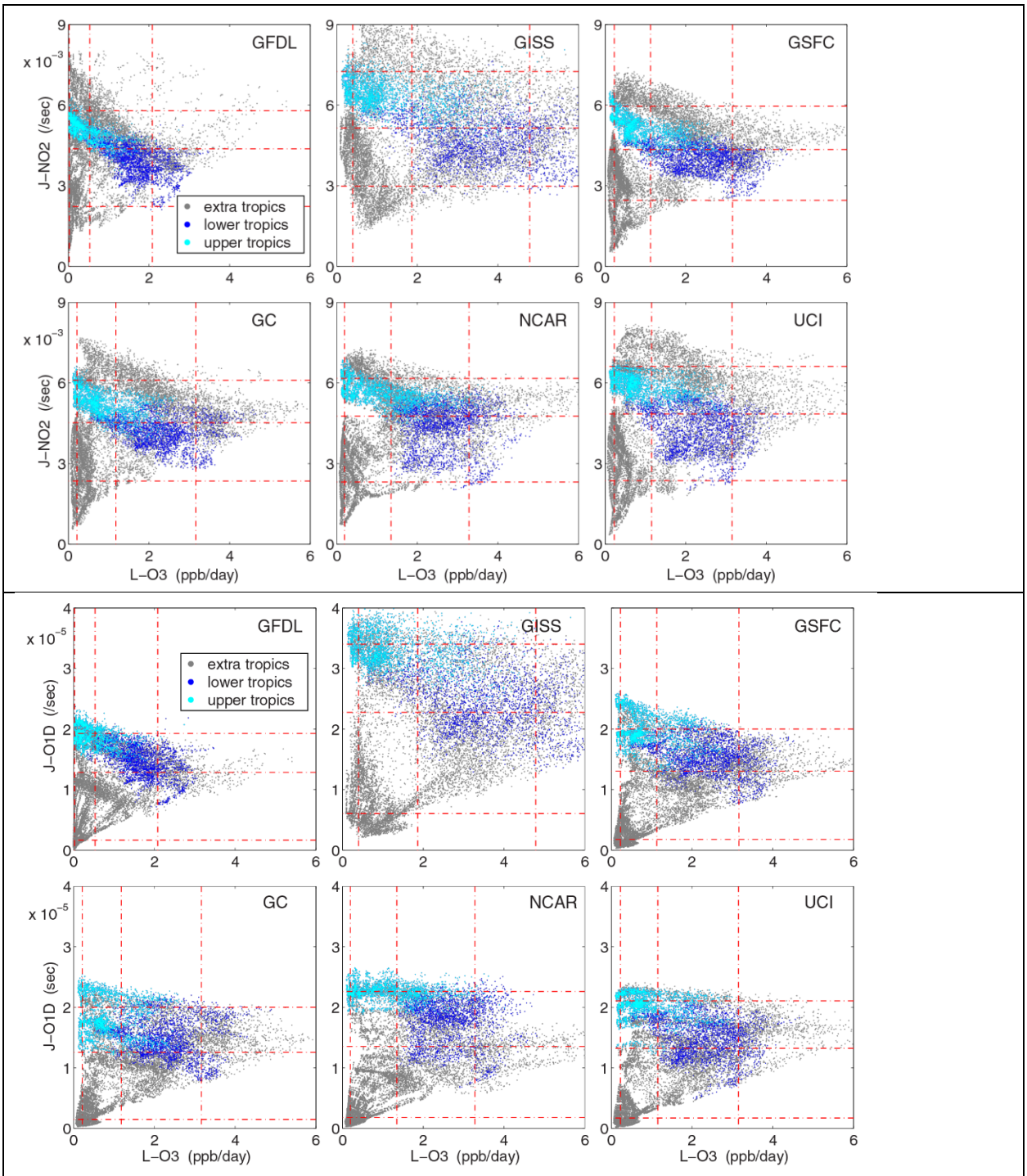

Figure S4. Parcel values of (top) J-NO2 and (bottom) J-O1D vs. L-O3 for each of the models. See Figure 1.

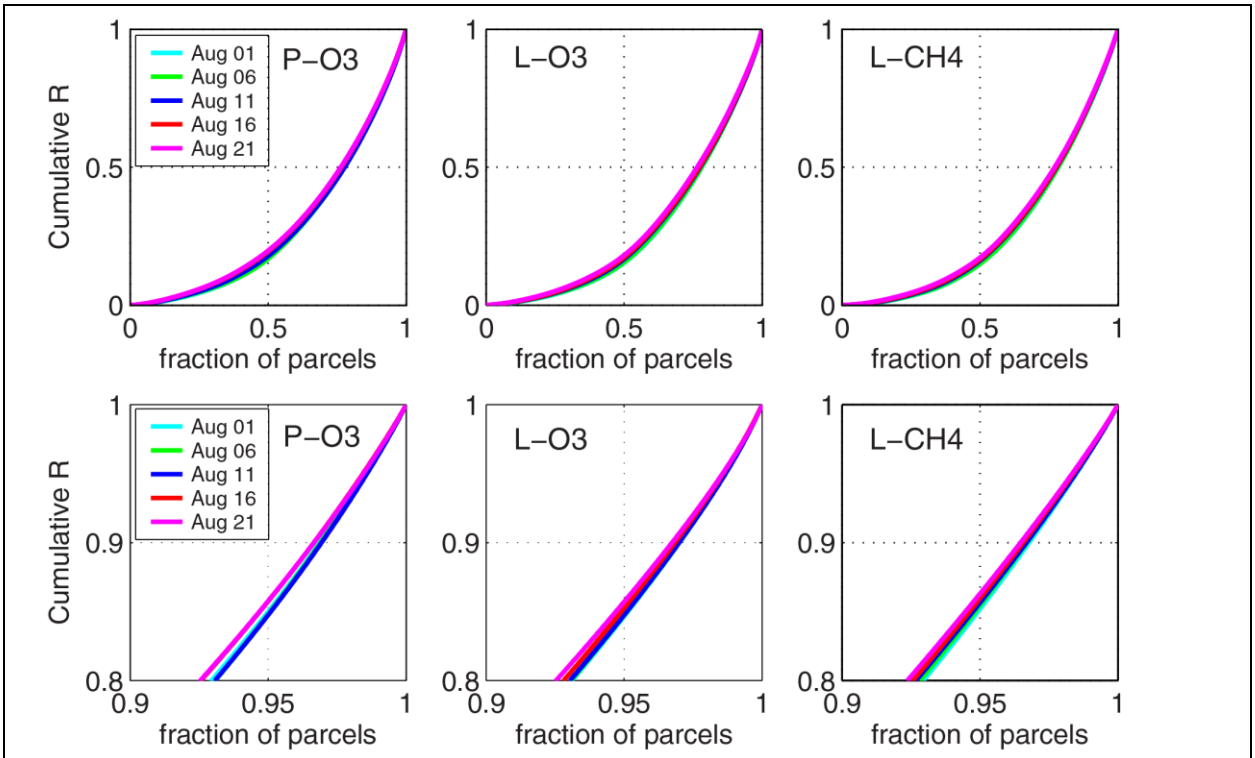

Figure S5. Cumulative reactivity of the 14,880 parcels (equally weighted) scaled to the average of each model day and reactivity. The lower panel shows a blowup of the top 20% (Cumulative = 0.8 to 1.0). Results for the 5 days in August for UCI.

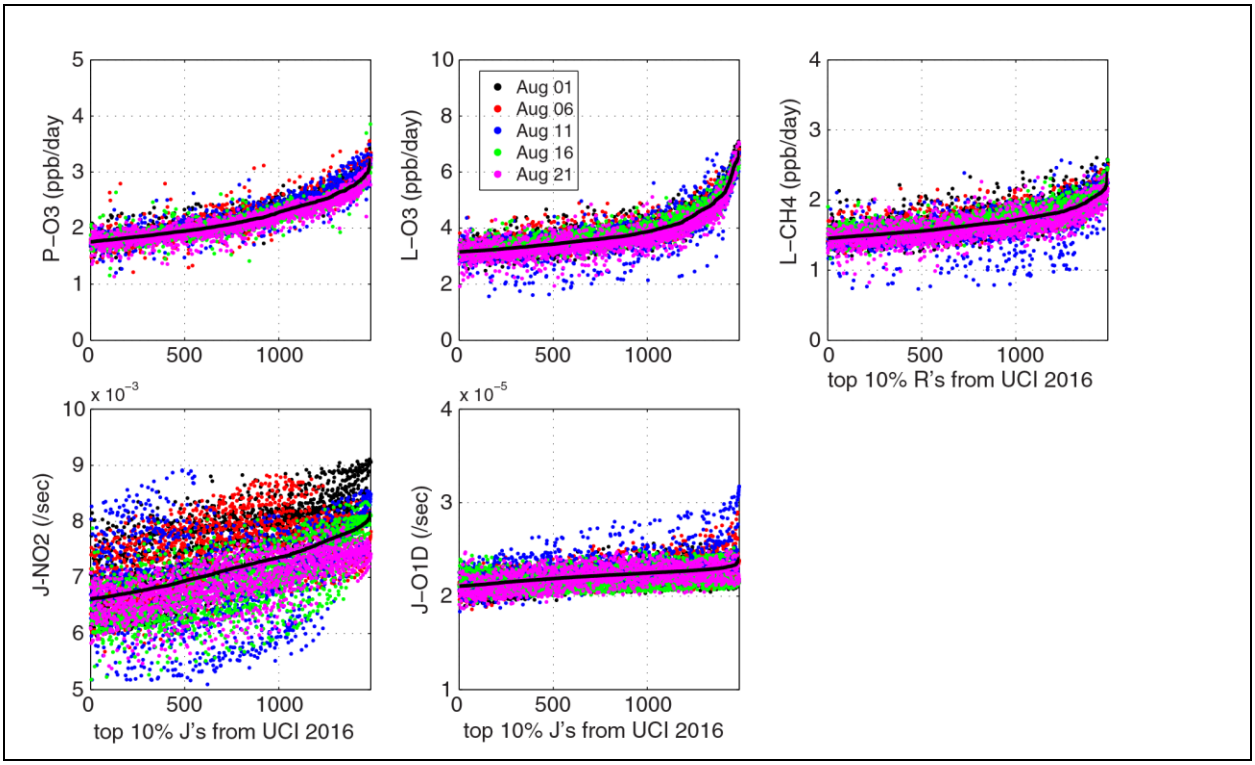

Figure S6. Modeled Reactivity and J-values of the top-10% parcels for 5 separate days for UCI, sorted by and plotted against the 5-day mean (black line). See figure S8.

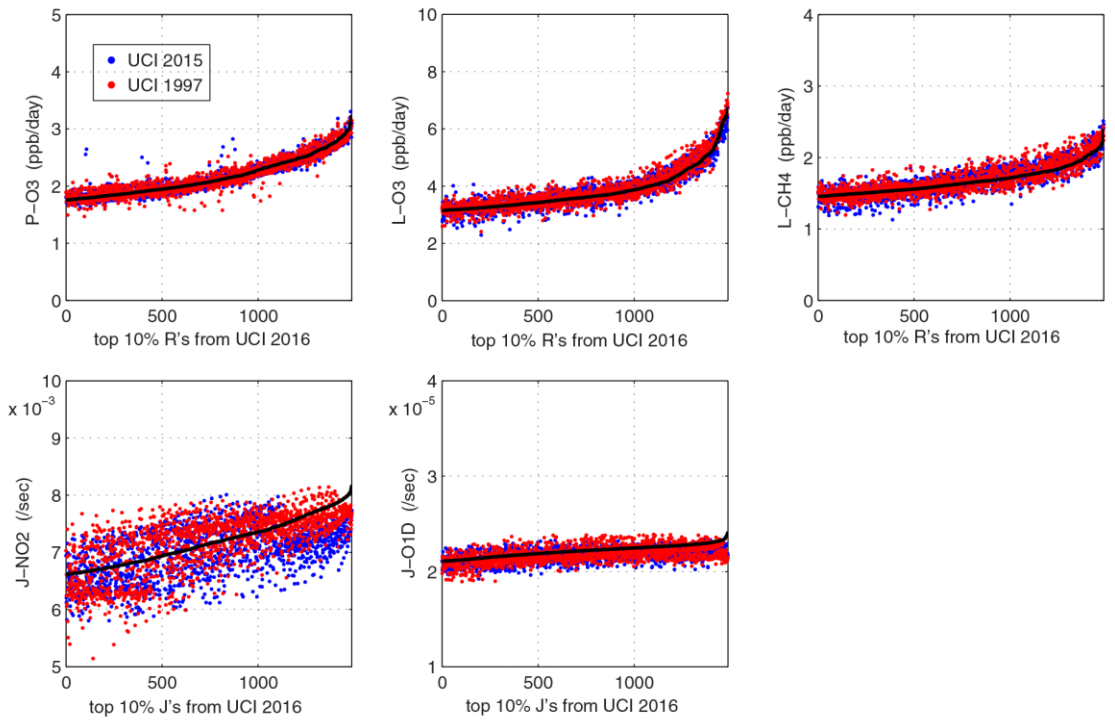

Figure S7. Modeled Reactivity and J-values of the top-10% parcels (all 5-day means) from two different years with UCI (1997, 2015), sorted by and plotted against the standard UCI model (year 2016, black line). See figure S8.

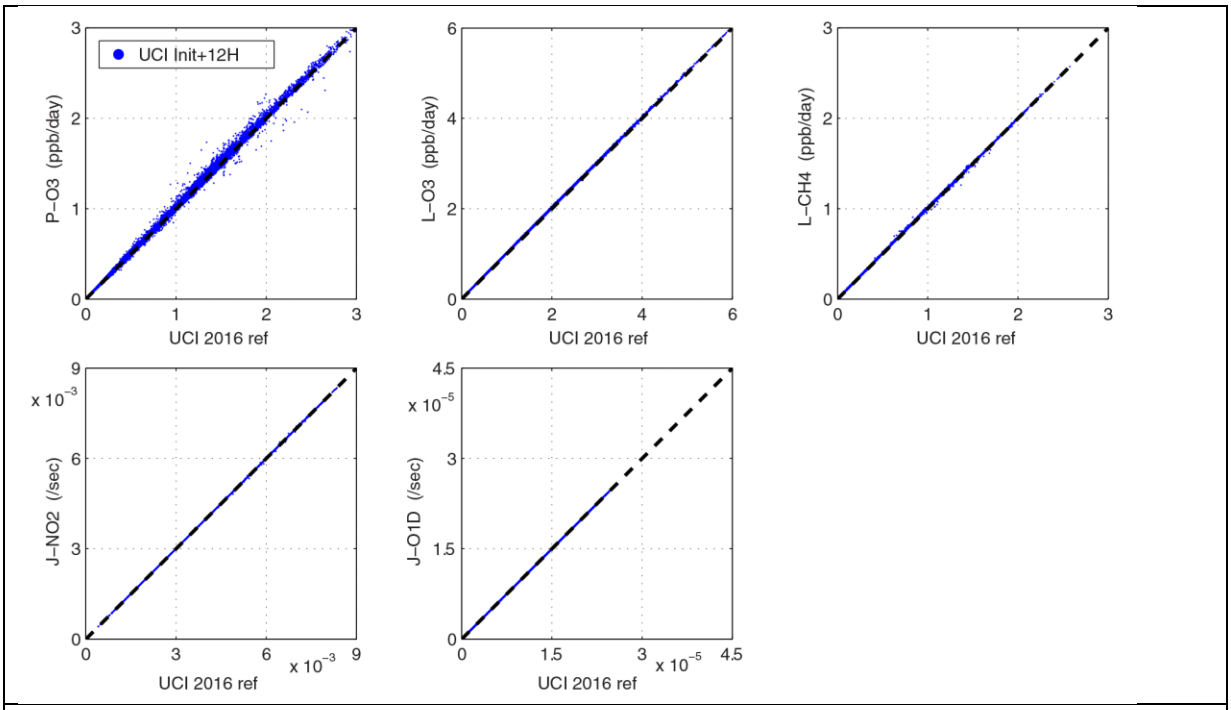

Figure S8. Scatter plot of reactivities and J-values for a single day (2016/08/16) using the UCI model initiating the calculation 12 hours later at 0000H instead of 1200H, but maintaining the same cloud fields at each solar zenith angle.

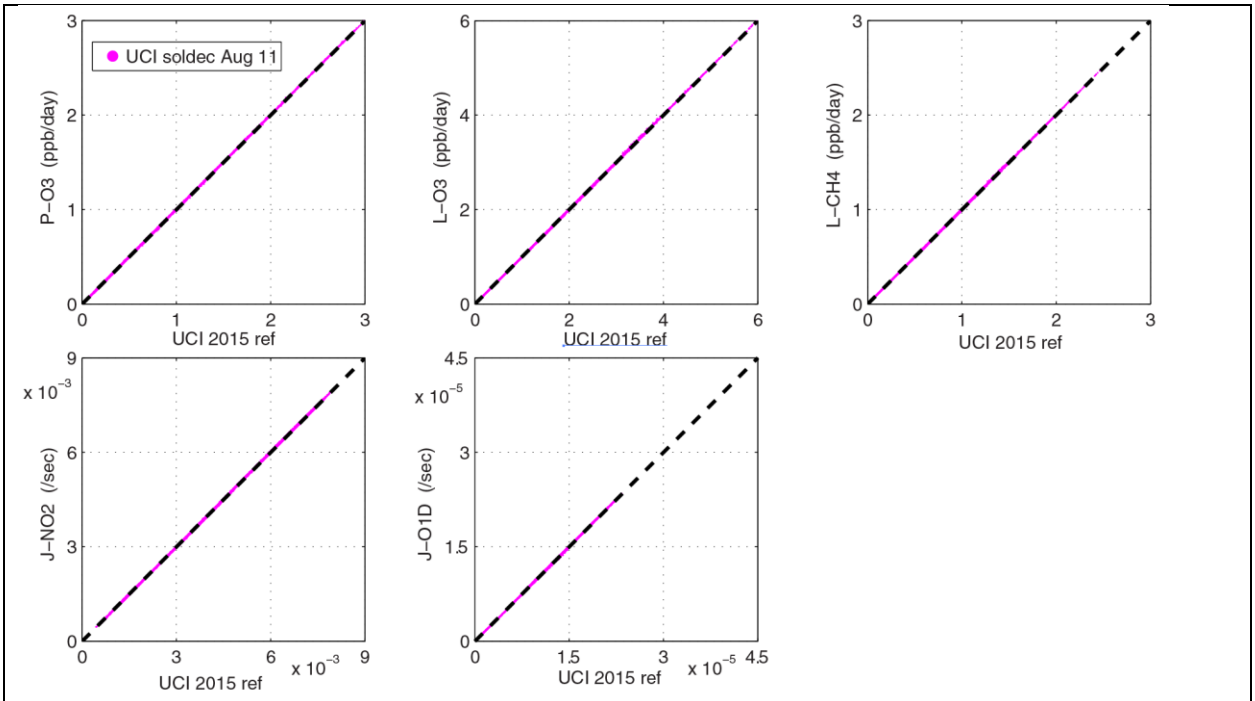

Figure S9. Scatter plot of reactivities and J-values for 5d-mean air parcels from the UCI model reference year 2015 holding the seasonal change in solar declination fixed at Aug 11 values instead of varying over the 5 different days from Aug 1 to Aug 21.

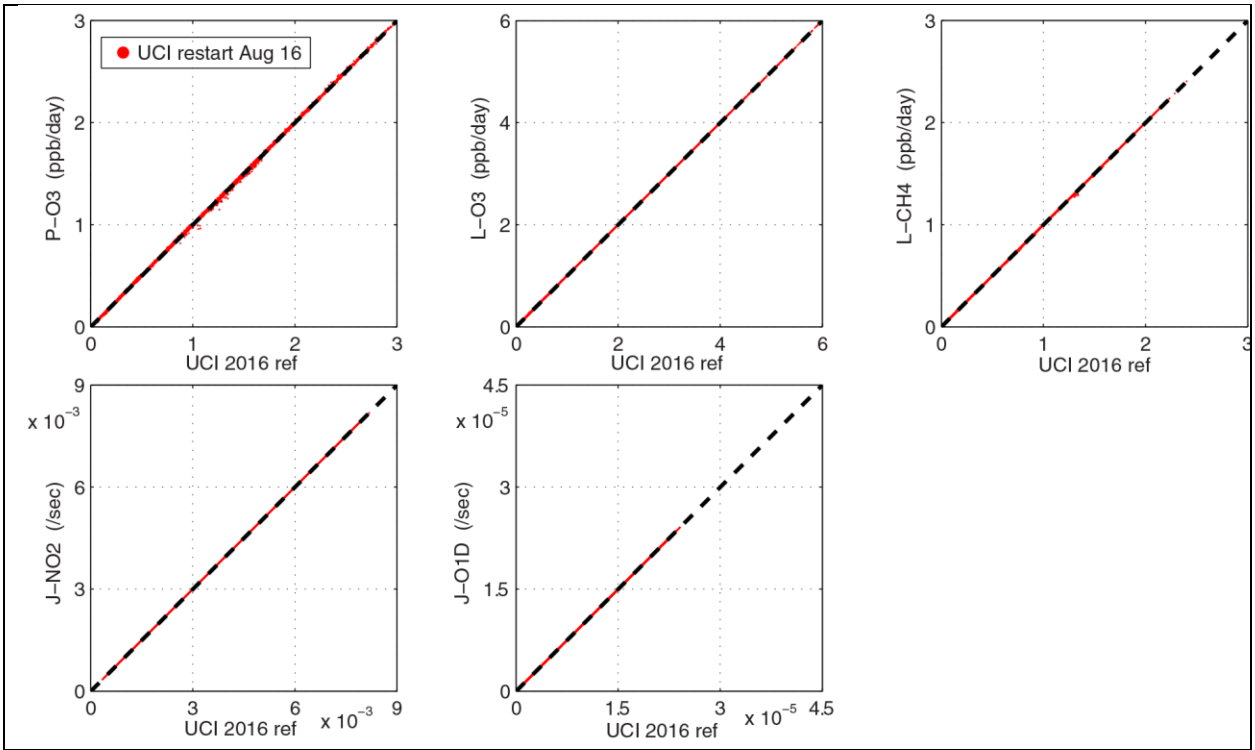

Figure S10. Scatter plot of reactivities and J-values for 5d-mean air parcels from the UCI model using a different restart file from Aug 16 instead of the reference Aug 11 (but with the same data stream parcels).

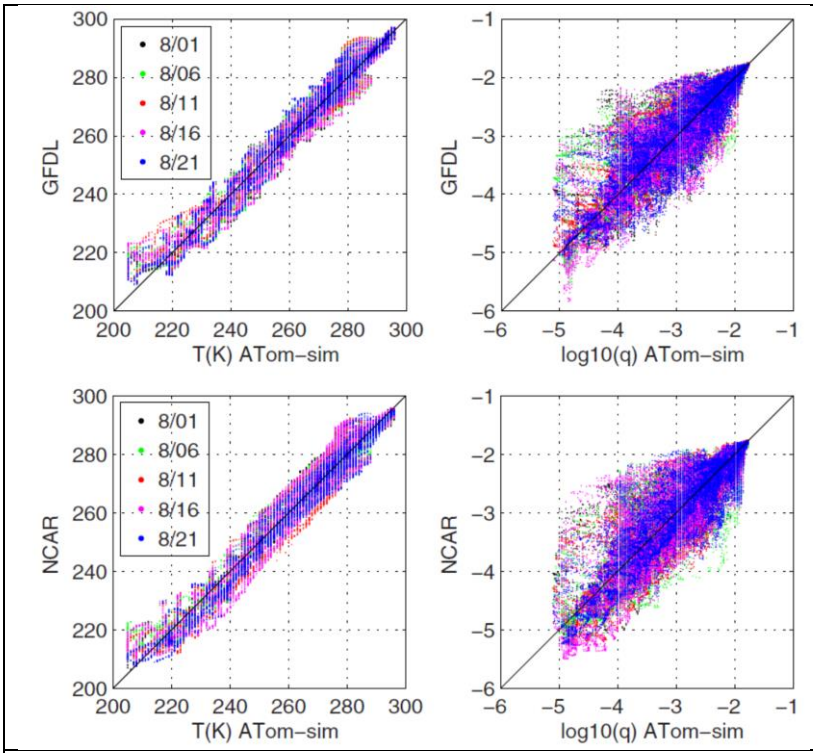

Figure S11. Scatter plot of the GFDL and NCAR T&q values used in their calculations vs the specified data stream for the 14,880 parcels.

References

ATom: Measurements and modeling results from the NASA Atmospheric Tomography Mission, https://espoarchive.nasa.gov/archive/browse/atom, doi: 10.5067/Aircraft/ATom/TraceGas_Aerosol_Global_Distribution, 2017.

Batchelor, G. K.: The Effect of Homogeneous Turbulence on Material Lines and Surfaces, Proc. R. Soc. Lond. A 1952 213 349-366; DOI: 10.1098/rspa.1952.0130, 1952.

Brasseur, G. P., D. A. Hauglustaine, S. Walters, P. J. Rasch, J.-F. Müller, C. Granier, and X. X. Tie: MOZART, a global chemical transport model for ozone and related chemical tracers: 1. Model description, J. Geophys. Res., 103(D21), 28265–28289, doi:10.1029/98JD02397, 1998.

Collins, W. J., Lamarque, J. F., Schulz, M., Boucher, O., Eyring, V., Hegglin, M. I., Maycock, A., Myhre, G., Prather, M., Shindell, D., and Smith, S. J.: AerChemMIP: quantifying the effects of chemistry and aerosols in CMIP6, Geosci Model Dev, 10, 585-607, 10.5194/gmd-10-585-2017, 2017.

Duncan, B.N., S.E. Strahan, Y. Yoshida, S.D. Steenrod, and N. Livesey: Model study of cross-tropopause transport of biomass burning pollution, Atmos. Chem. Phys., 7, 3713-3736, 2007.

Eyring, V., N. Butchart, D. W. Waugh, H. Akiyoshi, J. Austin, S. Bekki, G. E. Bodeker, B. A. Boville, C. Brühl, M. P. Chipperfield, E. Cordero, M. Dameris, M. Deushi, V. E. Fioletov, S. M. Frith, R. R. Garcia, A. Gettelman, M. A. Giorgetta, V. Grewe, L. Jourdain, D. E. Kinnison, E. Mancini, E. Manzini, M. Marchand, D. R. Marsh, T. Nagashima, P. A. Newman, J. E. Nielsen, S. Pawson, G. Pitari, D. A. Plummer, E. Rozanov, M. Schraner, T. G. Shepherd, K. Shibata, R. S. Stolarski, H. Struthers, W. Tian, M. Yoshiki: Assessment of temperature, trace species, and ozone in chemistry-climate model simulations of the recent past, J Geophys Res-Atmos, 111, -, Artn D22308 Doi 10.1029/2006jd007327, 2006.

Gelaro, Ronald, Will McCarty, Max J. Suárez, Ricardo Todling, Andrea Molod, Lawrence Takacs, Cynthia A. Randles, Anton Darmenov, Michael G. Bosilovich, Rolf Reichle, Krzysztof Wargan, Lawrence Coy, Richard Cullather, Clara Draper, Santha Akella, Virginie Buchard, Austin Conaty, Arlindo M. da Silva, Wei Gu, Gi-Kong Kim, Randal Koster, Robert Lucchesi, Dagmar Merkova, Jon Eric Nielsen, Gary Partyka, Steven Pawson, William Putman, Michele Rienecker, Siegfried D. Schubert, Meta Sienkiewicz, and Bin Zhao: The Modern-Era Retrospective Analysis for Research and Applications, Version 2 (MERRA-2), J Climate, 30(14), 5419–5454, doi:10.1175/JCLI-D-16-0758.1, 2017

Holmes, C.D., M. J. Prather, A.O. Søvde, G. Myhre: Future methane, hydroxyl, and their uncertainties: key climate and emission parameters for future predictions, Atmos. Chem. Phys., 13, 285–302, doi:10.5194/acp-13-285-2013, 2013.

Horowitz, L. W., Stacy Walters, Denise L. Mauzerall, Louisa K. Emmons, Philip J. Rasch, Claire Granier, XueXi Tie, Jean-François Lamarque, Martin G. Schultz, Geoffrey S. Tyndall, John J. Orlando, Guy P. Brasseur: A global simulation of tropospheric ozone and related tracers: Description and evaluation of MOZART, version 2, J. Geophys. Res., 108(D24), 4784, doi:10.1029/2002JD002853, 2003.

Houweling, S., Dentener, F., and Lelieveld, J.: The impact of non- methane hydrocarbon compounds on tropospheric photochemistry, J. Geophys. Res., 103, 10673–10696, 1998.

Lauritzen, P. H., Ullrich, P. A., Jablonowski, C., Bosler, P. A., Calhoun, D., Conley, A. J., Enomoto, T., Dong, L., Dubey, S., Guba, O., Hansen, A. B., Kaas, E., Kent, J., Lamarque, J. F., Prather, M. J., Reinert, D., Shashkin, V. V., Skamarock, W. C., Sorensen, B., Taylor, M. A., and Tolstykh, M. A.: A standard test case suite for two-dimensional linear transport on the sphere: results from a collection of state-of-the-art schemes, Geosci Model Dev, 7, 105-145, 10.5194/gmd-7-105-2014, 2014.

Li, J., Mao, J., Fiore, A. M., Cohen, R. C., Crounse, J. D., Teng, A. P., Wennberg, P. O., Lee, B. H., Lopez-Hilfiker, F. D., Thornton, J. A., Peischl, J., Pollack, I. B., Ryerson, T. B., Veres, P., Roberts, J. M., Neuman, J. A., Nowak, J. B., Wolfe, G. M., Hanisco, T. F., Fried, A., Singh, H. B., Dibb, J., Paulot, F., and Horowitz, L. W.: Decadal change of summertime reactive nitrogen species and surface ozone over the Southeast United States, Atmos. Chem. Phys. Discuss., https://doi.org/10.5194/acp-2017-606, 2017.

Madronich, S.: Photodissociation in the atmosphere: 1. Actinic flux and the effect of ground reflections and clouds, J. Geophys. Res., 92, 9740 – 9752, 1987.

Morgenstern, O., Hegglin, M. I., Rozanov, E., O'Connor, F. M., Abraham, N. L., Akiyoshi, H., Archibald, A. T., Bekki, S., Butchart, N., Chipperfield, M. P., Deushi, M., Dhomse, S. S., Garcia, R. R., Hardiman, S. C., Horowitz, L. W., Jockel, P., Josse, B., Kinnison, D., Lin, M. Y., Mancini, E., Manyin, M. E., Marchand, M., Marecal, V., Michou, M., Oman, L. D., Pitari, G., Plummer, D. A., Revell, L. E., Saint-Martin, D., Schofield, R., Stenke, A., Stone, K., Sudo, K., Tanaka, T. Y., Tilmes, S., Yamashita, Y., Yoshida, K., and Zeng, G.: Review of the global models used within phase 1 of the Chemistry-Climate Model Initiative (CCMI), Geosci Model Dev, 10, 639-671, 10.5194/gmd-10-639-2017, 2017.

Myhre, G., Aas, W., Cherian, R., Collins, W., Faluvegi, G., Flanner, M., Forster, P., Hodnebrog, O., Klimont, Z., Lund, M. T., Mulmenstadt, J., Myhre, C. L., Olivie, D., Prather, M., Quaas, J., Samset, B. H., Schnell, J. L., Schulz, M., Shindell, D., Skeie, R. B., Takemura, T., and Tsyro, S.: Multi-model simulations of aerosol and ozone radiative forcing due to anthropogenic emission changes during the period 1990-2015, Atmos Chem Phys, 17, 2709-2720, 10.5194/acp-17-2709-2017, 2017.

NAP, Causes and Effects of Changes in Stratospheric Ozone: Update 1983, ISBN 0-309-03443-4, National Academy Press, Washington DC, 1984.

NASA, Report of the 1992 Stratospheric Models and Measurements Workshop, (Prather, M.J. and E.E. Remsberg, eds.), Satellite Beach, FL, February 1992, NASA Ref. Publ. 1292, 144+268+352 pp., 1993.

Nault, B. A., Garland, C., Wooldridge, P. J., Brune, W. H., Campuzano-Jost, P., Crounse, J. D., Day, D. A., Dibb, J., Hall, S. R., Huey, L. G., Jimenez, J. L., Liu, X. X., Mao, J. Q., Mikoviny, T., Peischl, J., Pollack, I. B., Ren, X. R., Ryerson, T. B., Scheuer, E., Ullmann, K., Wennberg, P. O., Wisthaler, A., Zhang, L., and Cohen, R. C.: Observational Constraints on the Oxidation of NOx in the Upper Troposphere, J Phys Chem A, 120, 1468-1478, 10.1021/acs.jpca.5b07824, 2016.

Olson, J. R., Crawford, J. H., Brune, W., Mao, J., Ren, X., Fried, A., Anderson, B., Apel, E., Beaver, M., Blake, D., Chen, G., Crounse, J., Dibb, J., Diskin, G., Hall, S. R., Huey, L. G., Knapp, D., Richter, D., Riemer, D., Clair, J. S., Ullmann, K., Walega, J., Weibring, P., Weinheimer, A., Wennberg, P., and Wisthaler, A.: An analysis of fast photochemistry over high northern latitudes during spring and summer using in-situ observations from ARCTAS and TOPSE, Atmos Chem Phys, 12, 6799-6825, 10.5194/acp-12-6799-2012, 2012.

Olson, J., Prather, M., Berntsen, T., Carmichael, G., Chatfield, R., Connell, P., Derwent, R., Horowitz, L., Jin, S. X., Kanakidou, M., Kasibhatla, P., Kotamarthi, R., Kuhn, M., Law, K., Penner, J., Perliski, L., Sillman, S., Stordal, F., Thompson, A., and Wild, O.: Results from the Intergovernmental Panel on Climatic Change Photochemical Model Intercomparison (PhotoComp), J Geophys Res-Atmos, 102, 5979-5991, 1997.

Orbe, C., Waugh, D. W., Newman, P. A., and Steenrod, S.: The Transit-Time Distribution from the Northern Hemisphere Midlatitude Surface, J Atmos Sci, 73, 3785-3802, 10.1175/Jas-D-15-0289.1, 2016.

PhotoComp: Chapter 6 - Stratospheric Chemistry SPARC Report No. 5 on the Evaluation of Chemistry-Climate Models, World Meteorological Organization, Geneva, Switzerland, 194-202, 2010.

Prather, M. J., Zhu, X., Flynn, C. M., Strode, S. A., Rodriguez, J. M., Steenrod, S. D., Liu, J. H., Lamarque, J. F., Fiore, A. M., Horowitz, L. W., Mao, J. Q., Murray, L. T., Shindell, D. T., and Wofsy, S. C.: Global atmospheric chemistry - which air matters, Atmos Chem Phys, 17, 9081-9102, 10.5194/acp-17-9081-2017, 2017.

Prather, M., C. Flynn, A. Fiore, G. Correa, S.A. Strode, S. Steenrod, L. Murray, and J-F. Lamarque:. ATom: Simulated Data Stream for Modeling ATom-like Measurements. ORNL DAAC, Oak Ridge, Tennessee, USA. https://doi.org/10.3334/ORNLDAAC/1597, 2018.

Prather, M. J., Zhu, X., Strahan, S. E., Steenrod, S. D., and Rodriguez, J. M.: Quantifying errors in trace species transport modeling, P Natl Acad Sci USA, 105, 19617-19621, DOI 10.1073/pnas.0806541106, 2008.

Prather, M. J.: Photolysis rates in correlated overlapping cloud fields: Cloud-J 7.3c, Geosci Model Dev, 8, 2587-2595, 10.5194/gmd-8-2587-2015, 2015.

Prather, M., and Jaffe, A. H.: Global Impact of the Antarctic Ozone Hole - Chemical Propagation, J Geophys Res-Atmos, 95, 3473-3492, 1990.

Prather, M.J., J. Hsu (2010), Coupling of nitrous oxide and methane by global atmospheric chemistry, Science, 330: 952-954.

Rienecker, M. M., Max J. Suarez, Ronald Gelaro, Ricardo Todling, Julio Bacmeister, Emily Liu, Michael G. Bosilovich, Siegfried D. Schubert, Lawrence Takacs, Gi-Kong Kim, Stephen Bloom, Junye Chen, Douglas Collins, Austin Conaty, Arlindo da Silva, Wei Gu, Joanna Joiner, Randal D. Koster, Robert Lucchesi, Andrea Molod, Tommy Owens, Steven Pawson, Philip Pegion, Christopher R. Redder, Rolf Reichle, Franklin R. Robertson, Albert G. Ruddick, Meta Sienkiewicz, and Jack Woollen: MERRA: NASA's Modern-Era Retrospective Analysis for Research and Applications, J Climate, 24(14), 3624–3648, doi:10.1175/JCLI-D-11-00015.1, 2011.

Shindell, D. T. et al.:Interactive ozone and methane chemistry in GISS-E2 historical and future climate simulations, Atmos Chem Phys, 13(5), 2653–2689, doi:10.5194/acp-13-2653-2013, 2013.

Shindell, D., Kuylenstierna, J. C. I., Vignati, E., van Dingenen, R., Amann, M., Klimont, Z., Anenberg, S. C., Muller, N., Janssens-Maenhout, G., Raes, F., Schwartz, J., Faluvegi, G., Pozzoli, L., Kupiainen, K., Hoglund-Isaksson, L., Emberson, L., Streets, D., Ramanathan, V., Hicks, K., Oanh, N. T. K., Milly, G., Williams, M., Demkine, V., and Fowler, D.: Simultaneously Mitigating Near-Term Climate Change and Improving Human Health and Food Security, Science, 335, 183-189, DOI 10.1126/science.1210026, 2012.

Strahan, S.E., A.R. Douglass, and P.A. Newman: The contributions of chemistry and transport to low Arctic ozone in March 2011 derived from Aura MLS Observations, J. Geophys. Res., 118, 1563-1576, doi:10.1002/jgrd.50181, 2013.

Tilmes, S., Lamarque, J.-F., Emmons, L. K., Kinnison, D. E., Marsh, D., Garcia, R. R., Smith, A. K., Neely, R. R., Conley, A., Vitt, F., Val Martin, M., Tanimoto, H., Simpson, I., Blake, D. R., and Blake, N.: Representation of the Community Earth System Model (CESM1) CAM4-chem within the Chemistry-Climate Model Initiative (CCMI), Geosci. Model Dev., 9, 1853-1890, https://doi.org/10.5194/gmd-9-1853-2016, 2016.

Wild, O., Zhu, X., and Prather, M. J.: Fast-J: Accurate simulation of in- and below-cloud photolysis in tropospheric chemical models, J Atmos Chem, 37, 245-282, 2000.